

11-2022

## Interband Transitions and Critical Points of Single-Crystal Thoria Compared with Urania

Christina Dugan

Lu Wang

Kai Zhang

James M. Mann

Martin M. Kimani

*See next page for additional authors*

Follow this and additional works at: <https://scholar.afit.edu/facpub>



Part of the [Engineering Physics Commons](#)

---

### Recommended Citation

Dugan, C., Wang, L., Zhang, K., Mann, J. M., Kimani, M. M., Mei, W.-N., Dowben, P. A., & Petrosky, J. (2022). Interband transitions and critical points of single-crystal thoria compared with urania. *Physica Status Solidi (b)*, 259(11), 2200238. <https://doi.org/10.1002/pssb.202200238>

This Article is brought to you for free and open access by AFIT Scholar. It has been accepted for inclusion in Faculty Publications by an authorized administrator of AFIT Scholar. For more information, please contact [AFIT.ENWL.Repository@us.af.mil](mailto:AFIT.ENWL.Repository@us.af.mil).

---

## Authors

Christina Dugan, Lu Wang, Kai Zhang, James M. Mann, Martin M. Kimani, Wai-Ning Mei, Peter A. Dowben, and James C. Petrosky

# Interband Transitions and Critical Points of Single-Crystal Thoria Compared with Urania

Christina Dugan, Lu Wang, Kai Zhang, James Matthew Mann, Martin M. Kimani, Wai-Ning Mei,\* Peter A. Dowben, and James Petrosky

The interband transitions of  $\text{UO}_2$  are validated independently through cathode luminescence. A picture emerges consistent with density functional theory. While theory is generally consistent with experiment, it is evident from the comparison of  $\text{UO}_2$  and  $\text{ThO}_2$  that the choice of functional can significantly alter the bandgap and some details of the band structure, in particular at the conduction band minimum. Strictly *ab initio* predictions of the optical properties of the actinide compounds, based on density functional theory alone, continue to be somewhat elusive.

## 1. Introduction

The electronic properties of actinide dioxides, from  $\text{UO}_2$  to  $\text{AmO}_2$ , include the localized  $5f$  electronic states, where

C. Dugan, J. Petrosky  
Department of Engineering Physics  
Air Force Institute of Technology  
2950 Hobson Way, Wright-Patterson Air Force Base, OH 45433-7765, USA


L. Wang, K. Zhang  
CAS Key Lab of Materials for Energy Conversion  
Department of Materials Science and Engineering  
University of Science and Technology of China  
Hefei, Anhui 230026, China

J. M. Mann  
Air Force Research Laboratory  
Wright-Patterson Air Force Base, OH 45433-7765, USA

M. M. Kimani  
KBRwyle Technology Solutions  
Kellogg Brown & Root (KBR)  
Dayton, OH 45431, USA

W.-N. Mei  
Department of Physics  
University of Nebraska at Omaha  
60th and Dodge Streets, Omaha, NE 68182-0266, USA  
E-mail: physmei@unomaha.edu

P. A. Dowben  
Department of Physics and Astronomy  
University of Nebraska-Lincoln  
Theodore Jorgensen Hall, 855 North 16th Street, Lincoln, NE 68588-0299, USA

 The ORCID identification number(s) for the author(s) of this article can be found under <https://doi.org/10.1002/pssb.202200238>.

© 2022 The Authors. *physica status solidi (b) basic solid state physics* published by Wiley-VCH GmbH. This is an open access article under the terms of the Creative Commons Attribution License, which permits use, distribution and reproduction in any medium, provided the original work is properly cited.

DOI: 10.1002/pssb.202200238

application of a strong on-site Coulomb repulsion interaction is typically required in density functional theory (DFT) calculations.<sup>[1–27]</sup> As insulators, the  $5f$ -to- $f$  transitions are less perturbed by band hybridization in the actinide dioxides, but band hybridization remains significant. While an accurate quantitative description of the optical spectra requires theory beyond the independent particle picture, qualitative agreement between theory and experiment can often be obtained on the level of

DFT,<sup>[7,10,11,13–18]</sup> although there is wide variability in the predictions available from theory.<sup>[10,15]</sup> While the optical adsorption and reflectance spectra of semiconductors have been studied for several decades, similar work on actinide dioxides has been hampered by the absence of high-quality single crystals<sup>[10,28,29]</sup> as defects abound<sup>[10]</sup> affecting the experimental optical absorption. This presents challenges to efforts to experimentally verify the best theoretical approach. While the optical properties for both  $\text{ThO}_2$ <sup>[15]</sup> and  $\text{UO}_2$ <sup>[10,12,15,17,18]</sup> have been previously calculated using the Heyd–Scuseria–Ernzerhof (HSE) functional, even within the framework of the same functional, the bandgap can vary by as much as 22–27% for  $\text{UO}_2$ , so experimental verification from crystals free of defects becomes important.

The complex dielectric function  $\epsilon(\omega) = \epsilon_1(\omega) + i\epsilon_2(\omega)$  has been derived experimentally from  $\text{UO}_2$  single crystals, along with the roughly 2 eV bandgap, optically.<sup>[30–32]</sup> More recent efforts to extract the complex dielectric function have been made by Siekhaus and J. Crowhurst<sup>[24]</sup> as well as Mock, Dugan, and coworkers.<sup>[13,14]</sup> There are significant shifts in the transitions observed in the more recent optical ellipsometry measurements<sup>[13,14,33]</sup> compared with reflectivity measurements performed by Schoenes.<sup>[30–32]</sup> Absorption of  $\text{UO}_2$  thin films, by optical transmission, has also been measured.<sup>[34]</sup> Uranium oxide and thorium oxide single crystals, fabricated using a hydrothermal synthesis growth technique,<sup>[13,14,35–41]</sup> produce bulk single crystals of near-stoichiometric  $\text{UO}_2$ <sup>[13,14,36,39–41]</sup> and  $\text{ThO}_2$ <sup>[14,33,37,38,41]</sup> so that defect contributions to the complex dielectric function are much suppressed.<sup>[14]</sup> These improved single  $\text{UO}_2$  crystals allow us here to validate the observed interband transitions identified in variable-angle ellipsometry (VASE)<sup>[13,14]</sup> with cathode luminescence and theory. There is much prior theory on  $\text{UO}_2$  upon which to draw,<sup>[1–27]</sup> so here there is a somewhat increased emphasis on  $\text{ThO}_2$  to provide an indication that, as in the case of  $\text{UO}_2$ ,<sup>[10,15]</sup> the choice of DFT functional leads to wide variability in quantities like bandgap that are extracted from the calculated band structure.

## 2. Theoretical Methods

All the electronic band structure calculations were performed within the framework of spin-polarized plane-wave density functional theory (PW-DFT), implemented in the Vienna ab initio simulation package (VASP).<sup>[42,43]</sup> The Perdew–Burke–Ernzerhof (PBE) functional and projector-augmented wave (PAW) potentials were used.<sup>[44–46]</sup> An energy cutoff of 600 eV was adopted for the planewave expansion of the electronic wave function. Geometrical structures were relaxed until the force on each atom is less than  $0.01 \text{ eV } \text{\AA}^{-1}$  and the energy convergence criteria of  $10^{-7} \text{ eV}$  were met. Here the  $\text{UO}_2$  and  $\text{ThO}_2$  stable structures are the fluorite structure (cubic space group  $Fm\bar{3}m$  (225)), as in previous work<sup>[13,14]</sup> and in most other DFT calculations.<sup>[1–27]</sup> This is a  $\text{UO}_2$  or  $\text{ThO}_2$  unit cell with four uranium atoms in face-centered cubic positions and eight oxygen atoms in the tetrahedral sites. Once the optimized structures were achieved, the hybrid functional, in the HSE06<sup>[47]</sup> form, was used to give more accurate bandgaps. The imaginary part of the frequency-dependent dielectric matrix was calculated based on the HSE06 ground states of  $\text{ThO}_2$  using random phase approximation (RPA).<sup>[48,49]</sup> The default  $U$  values for the uranium and thorium oxides are both 4 eV for  $f$ -electrons consistent with many other DFT calculations.<sup>[8,10,19–24,26,27]</sup> We note that in some previous ab initio studies of  $\text{UO}_2$  there is an expansion<sup>[50]</sup> or contraction<sup>[51]</sup> of the  $c$  lattice parameter, relative to the  $a$  and  $b$  lattice constants, leading to a tetragonal unit cell, and indicative of a different ground state<sup>[50]</sup> not seen here.

## 3. Interband Transitions of $\text{ThO}_2$ and $\text{UO}_2$

When the DFT +  $U$  method was used, with a choice of  $U = 4 \text{ eV}$  for  $f$ -states of Th atoms to provide the necessary correction for the on-site Coulomb interactions, the calculated bandgap is found to be 5.04 eV. Using the HSE functional to estimate a more accurate bandgap, as has been very popular with  $\text{UO}_2$ ,<sup>[9,10,12,13,15,17,18]</sup> our calculation revealed that the ground states of bulk  $\text{ThO}_2$  are non-magnetic, with a bandgap of 6.12 eV, as shown in **Figure 1**. This is close to the 6.21 eV value previously calculated.<sup>[15]</sup> It has also been shown that the HSE band structure calculations, with spin-orbit coupling turned on, provides a bandgap of 5.8 eV,<sup>[9,12]</sup> which is closer to the experimental value of 5.75 eV<sup>[52]</sup> and our value of 5.4 eV measured from VASE. The HSE functional does, however, differ significantly from the calculated band structure obtained using PBE, discussed below, and the band structures previously reported.<sup>[9,53]</sup>

These bandgaps are not representative nor do they include surface effects. Density functional theory slab calculations indicate that  $\text{ThO}_2(001)$ , with a Th atom termination, is not a spin-polarized semiconductor, and in this approach, we are left with the suggestion that the bandgap is small, of order 0.28 eV.  $\text{ThO}_2(100)$ , with an O atom termination, is a ferromagnetic metal with the magnetic moments of the supercell  $4.0 \mu_B$ . Basically, by including the surface, the  $\text{ThO}_2(001)$  band structure is characteristic of a semimetal, an  $n$ -type semimetal if the  $\text{ThO}_2(100)$  surface terminates with Th atoms and a  $p$ -type semimetal if the  $\text{ThO}_2(001)$  surface terminates with Th atoms. The semimetal bandgap has an indirect gap of about 2.7 eV, and in any case,

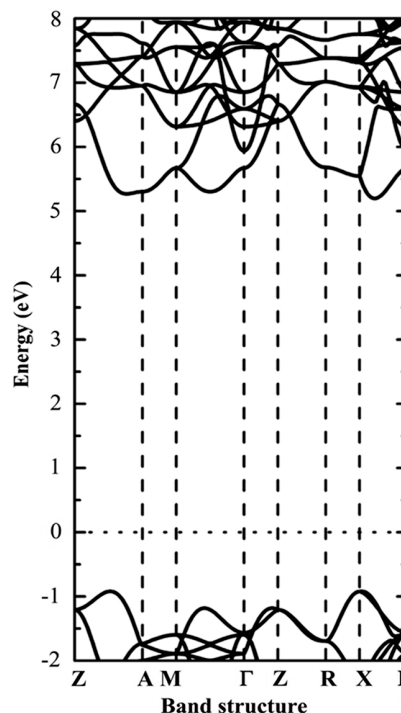


**Figure 1.** The band structure of bulk  $\text{ThO}_2$  using HSE hybrid functional. The bandgap is 6.12 eV and the ground state is antiferromagnetic.

the predicted semimetal behavior of the surface is not what has been measured optically.<sup>[14,52]</sup>

The PBE-calculated  $\text{ThO}_2$  band structure, with a correlation  $U = 4 \text{ eV}$ , as in **Figure 2**, is qualitatively similar to the band structure obtained through the B3LYP functional<sup>[9]</sup> and the relativistic linear augmented-planewave (RLAPW) calculation<sup>[53]</sup> for the valence band, but differs significantly from the calculated band structure, using the B3LYP functional or RLAPW, on the conduction band side. One difference with the calculated band structure of other studies,<sup>[9,53]</sup> and the calculations shown here, is that the calculation of **Figure 1** does have the conduction band minimum at the L point of the Brillouin zone, as shown in the study by Szpunar et al.,<sup>[9]</sup> but this is clearly not seen in **Figure 2** where the conduction band minimum is close to the K point. For the pure  $\text{ThO}_2$  bulk, the bandgap is 5.04 eV in the PBE +  $U$  functional, consistent with most other theory published to date.<sup>[9,12,15,53,54]</sup> A similar band gap was obtained with PBE +  $U$  in the density mixing scheme and the ensemble density functional theory (EDFT) scheme. These are the band structures within the same PBE functional plus a correlation energy  $U$  from different convergence schemes and should converge to the same ground states. While the band structure is very similar, one makes  $\text{ThO}_2$  more  $p$ -type and the other more  $n$ -type. A key point that comes from comparing the band structure from different functionals is that the resulting calculated band structures do differ.

Moving beyond the band structure calculations for  $\text{ThO}_2$  provided here and elsewhere,<sup>[9,12,14,15,53,54]</sup> we have calculated the bulk dielectric function, as shown in **Figure 3** for  $\text{ThO}_2$ . Absorption and the optical response will occur for any symmetry and selection rule allowed transition at any place in the Brillouin

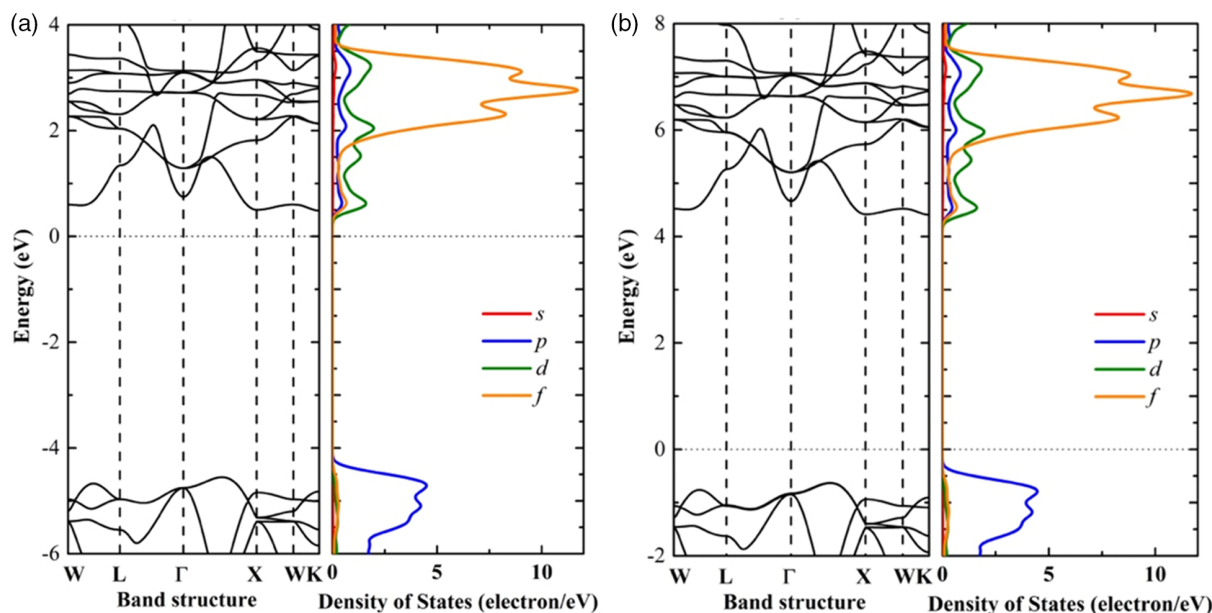


**Figure 2.** Band structure and density of states of ThO<sub>2</sub> by the a) PBE + U functional in the density mixing scheme and by b) PBE + U functional in the EDFT scheme.

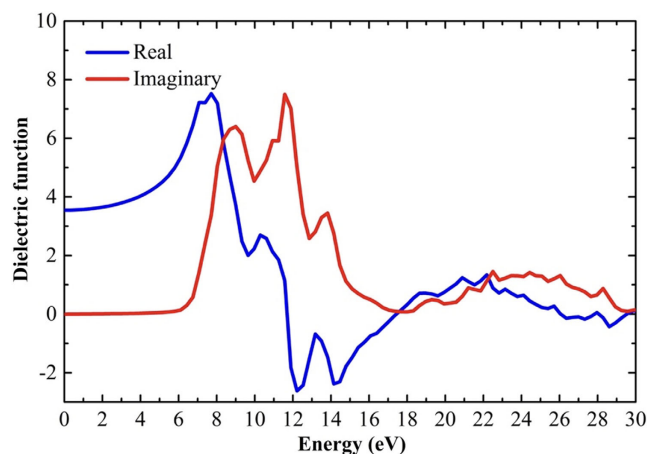


**Figure 3.** The calculated real (blue) and imaginary (red) parts of the ThO<sub>2</sub> dielectric function.

zone, not just  $\Gamma$ , so long the transition itself has little or no momentum exchange, that is,  $\Delta q = 0$  transition. Basically, the low-lying critical points seen in the VASE experiments of ThO<sub>2</sub><sup>[14]</sup> are qualitatively reproduced in theory, though shifted to higher energies in the HSE theory, as summarized in Table 1. For PBE, the agreement is more in line with experiment, but also qualitatively similar to HSE. This means that the strongest contributions to the optical properties for ThO<sub>2</sub> are the p-d transitions in the region of 5–8 eV. This places the low-lying critical points for ThO<sub>2</sub> at 5.5 eV (the  $\Delta q = 0$  [p to d;  $e$  symmetry] transition in the  $\varepsilon_2(\omega)$  part of the dielectric function for single-crystalline ThO<sub>2</sub> and the  $\Delta q = 0$  [p to d;  $a_1$  symmetry] transition in the region of the center of the Brillouin zone) and at 6.8 eV (the

**Table 1.** Critical point energies for ThO<sub>2</sub>, obtained from VASE compared with theory. The assignment based on prior theory<sup>[15]</sup> is given as well as that based on the band structure provided here [\*].

Experiment [eV] <sup>a)</sup>	Theory [eV] <sup>b)</sup>	Assignment
5.4	6.1	O 2p → Th 6d [*] O 2p → Th 5f <sup>[15]</sup>
6.3	7.2	O 2p → Th 6d <sup>[15]</sup>
7.5	7.7	O 2p → Th 6d <sup>[15]</sup>
8.0	9.0	O 2p → Th 5f <sup>[15]</sup>
8.8	—	—

<sup>a)</sup>Experimentally determined energy values from VASE, taken from Mock et al.<sup>[14]</sup>;

<sup>b)</sup>HSE theoretically determined energy values.

combined  $q = 0$  transitions [p to d;  $e$  symmetry] in the region of W and K of the Brillouin zone). These transitions are strongly O 2p → Th 6d/5f transitions for the most part, made possible by Th d-f hybridization (Figure 2) with more Th 6d weight in the final state for the transitions at lower energies and more and more Th 5f in the final state for the transitions at energies in the region of 8–9 eV. This assignment, based on the band structures of ThO<sub>2</sub> of Figure 1 and 2, differs from the O 2p → Th 5f assignment of Dugan et al.<sup>[15]</sup> O 2p → Th 6p is an allowed optical transition, while O 2p → Th 5f is not, although possible because of d-f hybridization as just noted.

Five critical points are observed in the investigated spectra for both of the actinide oxides UO<sub>2</sub> (Table 2) and ThO<sub>2</sub> (Table 1). The two actinides present with a very similar oscillator pattern that appears to be compressed and shifted to higher energy for ThO<sub>2</sub>, for the features below 10 eV. The imaginary part of

**Table 2.** Critical point energies for  $\text{UO}_2$ , obtained from VASE and cathode luminescence (CL), compared with theory. The assignments are based on prior theory.<sup>[30]</sup>

Experiment [eV] <sup>a)</sup>	VASE	Experiment [eV] <sup>b)</sup>	CL	Theory [eV] <sup>c)</sup>	Assignment
2.0		2.4		2.2	$\text{U } 5f \rightarrow \text{U } 5f^{[30]}$
2.6		2.6		3.5	$\text{U } 5f \rightarrow \text{U } 5f$
		2.9			
5.0		3.8		4.6	$\text{U } 5f \rightarrow \text{U } 6d$
6.3		6.1		6.0	$\text{O } 2p \rightarrow \text{U } 6d/5f^{[30]}$
6.9		6.8		6.9	$\text{O } 2p \rightarrow \text{U } 6d/5f^{[30]}$

<sup>a)</sup>Experimentally determined energy values from VASE, taken from Mock et al.<sup>[14]</sup>,

<sup>b)</sup>Transitions taken from cathode luminescence; <sup>c)</sup>HSE theoretically determined energy values.

the calculated dielectric response for  $\text{ThO}_2$  has the first major feature at 9 eV, as shown in Figure 3. In the dielectric response calculated from the experimental VASE,<sup>[14]</sup> the first low-energy peak appears at a lower energy of 8 eV, consistent with the fact that the HSE functional estimates a larger bandgap than is observed experimentally (Table 1).

In the case of  $\text{UO}_2$ , the dielectric response derived from the experimental VASE<sup>[13,14]</sup> has two peaks at low energy, at 2.0 and 5.0 eV, respectively. This is consistent with the optical bandgap of 2.0 eV previously reported.<sup>[30–32]</sup> These low-energy features are not as well resolved in theory, as seen in Figure 4, but as noted in the study by Dugan et al.,<sup>[13]</sup> the bandgaps generally agree with theory if the HSE functional is used, while the PBE functional grossly underestimates the bandgap (as discussed in detail in the study by Dugan et al.<sup>[13]</sup>). This is, however, highly variable as the bandgap of 2.71 eV was found using HSE with  $U = 4.5$  eV and  $J = 0.5$ ,<sup>[10]</sup> and an even larger band of 2.76 eV was also found with HSE,<sup>[17]</sup> much larger than the bandgap 2.4<sup>[12,18]</sup> and 2.19 eV<sup>[13]</sup> found elsewhere using the HSE functional. The peaks in the calculated imaginary part of the dielectric response for  $\text{UO}_2$  (Figure 4) appear only as higher-energy shoulders in experiment<sup>[14]</sup> and as weak features in the

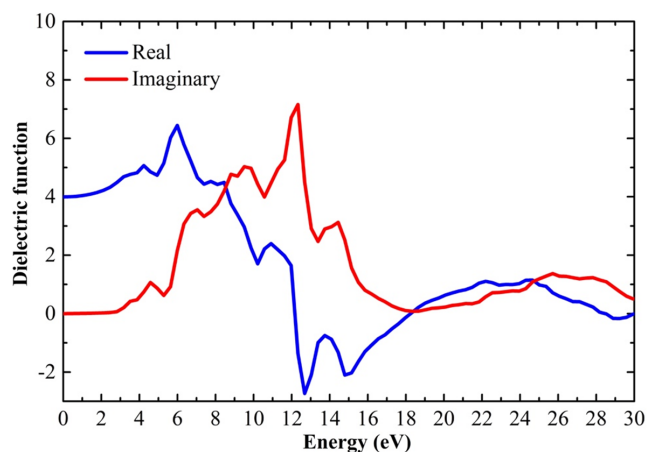


**Figure 4.** The calculated real (blue) and imaginary (red) parts of the  $\text{UO}_2$  dielectric function, using the HSE functional.

cathodoluminescence. This suggests that experiment and theory do not agree as to the extent of the oscillator strength used to describe the critical points' lower energies.

We observe also that the critical points seen in  $\text{UO}_2$  are broader than their counterparts in  $\text{ThO}_2$  in the imaginary part of the dielectric response extracted from the experimental VASE,<sup>[14]</sup> but the reverse is true in theory. These trends are seen in the calculated real and imaginary parts of the dielectric function for  $\text{ThO}_2$  (Figure 3) and  $\text{UO}_2$  (Figure 4). For the features at roughly 10, 12, 14, and 15 eV, thorium ( $\text{ThO}_2$ ) and urania ( $\text{UO}_2$ ) resemble each other as noted in the study by Dugan et al.<sup>[15]</sup> The calculated optical properties of Figure 3 and 4 differ, but it should be noted that there is now a wealth of information on  $\text{UO}_2$ , as shown in Table 2, and the transition energies in VASE previously measured<sup>[13,14]</sup> agree with the cathodoluminescence and theory. This means that the transitions can be assigned, based on the theory.

## 4. Cathodoluminescence

Figure 5 displays the cathodoluminescence, taken at 10 keV, for a single-crystalline  $\text{UO}_2$  sample grown by hydrothermal synthesis. The values given in Table 2 generally agree with the optical transition values extracted from the VASE.<sup>[13,14]</sup> An experimentally determined bandgap of 2.37 eV, from cathodoluminescence, is also consistent with theoretically predicted bandgaps of 2.19,<sup>[13]</sup> 2.3,<sup>[16]</sup> and 2.4 eV.<sup>[12]</sup> This value of 2.37 eV is larger than previously found by VASE (Table 1) and discussed at length in other studies.<sup>[13,14]</sup> As there is no initial state photohole, the luminescence corresponding to the lowest unoccupied state to highest occupied state transition is expected to be larger, as is the case with the value determined from VASE. The very low luminescence for the transitions corresponding to the bandgap is the result of being a selection rule forbidden transition.

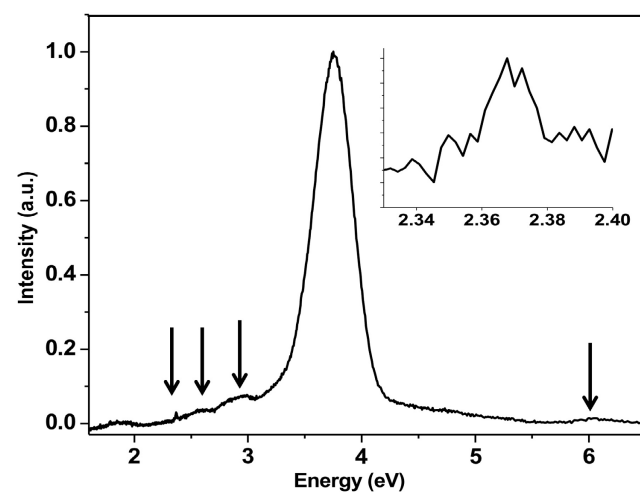


**Figure 5.** The optical transitions for single-crystal  $\text{UO}_2$ , measured from cathodoluminescence. The incident electron energy is 10 keV to avoid surface effects. The weaker transitions are indicated by arrows and that corresponding to the lowest unoccupied state to highest occupied state transition is shown in the inset.



The fact that the cathodoluminescence features are generally very weak, especially for the luminescence corresponding to the lowest unoccupied state to highest occupied state transition for single-crystal  $\text{UO}_2$ , is because this transition is a selection rule forbidden transition. A  $\text{U } 5f \rightarrow \text{U } 5f$  transition does not obey the required  $\Delta l = \pm 1$  for an optical transition, as noted in the discussion of the optical transitions above. The  $\text{U } 6d/5f \rightarrow \text{O } 2p$  luminescence transitions are also expected to be weak as they are extra-atomic transitions, as is observed here. As shown in Figure 5, the strongest luminescence feature is the on-site, selection rule allowed  $\text{U } 6d \rightarrow \text{U } 5f$  transition (the reverse of the transition in VASE previously measured<sup>[14]</sup>). This very strong cathodoluminescence feature at 3.8 eV appears at a lower energy than predicted by theory or seen in the VASE previously measured<sup>[14]</sup> or predicted by theory, indicative of extensive hybridization in the band structure. These transition assignments are, nonetheless, generally consistent not only with theory,<sup>[30]</sup> as noted earlier, but also combined photoemission and inverse photoemission studies of  $\text{UO}_2$ .<sup>[55]</sup> This, in turn, implies that  $\text{UO}_2$  and  $\text{ThO}_2$  are indeed strongly correlated systems with correlation energies in the region from 0<sup>[8]</sup> to 6 eV for  $\text{ThO}_2$ <sup>[7,9,25]</sup> and from 3.5 to 5 eV for  $\text{UO}_2$ .<sup>[8,10,19–24,26,27]</sup>

## 5. Conclusion

There is a consistent picture of the electronic structure, from experiment, that is not shared among the many theoretical band structure calculations. As noted elsewhere,<sup>[7,8,21,23,55]</sup> when it comes theory, the final arbiter of successful theoretical band structure calculations presently appears to be in agreement with the experiment results for the actinide oxides. As sample quality improves, the difference between experiments and theory is increasingly diminished, although the role of screening does appear to have a profound effect on the experiment. Surface effects, not discussed here, are expected to be a persistent problem and caution is needed in interpreting experimental results with a strong surface contribution. For example, the photoelectric work function of the (111) hydrothermally grown  $\text{UO}_2$  was measured at 3–4 eV,<sup>[39]</sup> and  $3.19 \pm 0.03$  eV.<sup>[27]</sup> More recently, the photoelectric determined work function of nearly stoichiometric hydrothermally grown  $\text{UO}_2(111)$  and (100) was measured to be  $6.28 \pm 0.36$  and  $5.80 \pm 0.36$  eV, respectively.<sup>[40]</sup> This range of experimental values reduces confidence in key parameters associated with these materials. However, as shown in this article, that confidence builds as theory and experiment begin to merge.

## 6. Experimental Section

Single crystals of  $\text{UO}_2$  were grown by hydrothermal synthesis,<sup>[13,14,35–41]</sup> as described in other studies.<sup>[13,14,41]</sup> Further, hydrothermal growth information is detailed in the study by Mann et al.<sup>[35]</sup> The  $\text{UO}_2$  crystals grown under these conditions have measured lattice parameters of  $5.4703 \pm 0.0006$  Å indicating a stoichiometry near  $\text{UO}_2$ .<sup>[25,56–59]</sup>

The cathodoluminescence system consists of a Kimball Physics EMG-12 electron gun powered by an EGPS-12 power supply, a vacuum system, a sample chamber with suitable optical ports, an optical system, a spectrometer, and a photomultiplier detector. The liquid nitrogen-cooled  $\text{UO}_2$  was placed at the focal point of the electron gun and the resulting

cathodoluminescence signal from the sample was transmitted through the quartz window of the vacuum chamber, focused onto the entrance slit of the monochromator and then to the photomultiplier or a solid-state detector. The electron beam was incident at an angle of  $\approx 45^\circ$  with 10 keV energy.

## Acknowledgements

This work was supported in part by the National Science Foundation under EPSCoR RII Track-1: Emergent Quantum Materials and Technologies (EQUATE), Award OIA-2044049 [W.-N.M., P.A.D.]. This work was also supported in part by the Air Force Office of Scientific Research under award FA9550-18-1-0360, by the Defense Threat Reduction Agency (grant no. HDTRA1-14-1-0041), and the Domestic Nuclear Detection Office of the Department of Homeland Security (grant no. HSHQDC14X00089). J.M.M. was supported by the Center for Thermal Energy Transport under Irradiation, an Energy Frontier Research Center funded by the U.S. Department of Energy, Office of Science, Office of Basic Energy Sciences. The views expressed in this article are those of the authors and do not reflect the official policy or position of the U.S. Air Force, Department of Defense, or the U.S. Government.

## Conflict of Interest

The authors declare no conflict of interest.

## Data Availability Statement

The data that support the findings of this study are available from the corresponding author upon reasonable request.

## Keywords

cathode luminescence, interband transitions, thorium, uranium

Received: May 31, 2022

Revised: July 28, 2022

Published online: August 26, 2022

- [1] J. C. Boettger, A. K. Ray, *Int. J. Quantum Chem.* **2000**, 80, 824.
- [2] J. C. Boettger, A. K. Ray, *Int. J. Quantum Chem.* **2002**, 90, 1470.
- [3] G. Jomard, B. Amadon, F. Bottin, M. Torrent, *Phys. Rev. B* **2008**, 78, 075125.
- [4] P. Zhang, B. T. Wang, X. G. Zhao, *Phys. Rev. B* **2010**, 82, 144110.
- [5] B. T. Wang, H. L. Shi, W. D. Li, P. Zhang, *Phys. Rev. B* **2010**, 81, 045119.
- [6] Y. Lu, Y. Yang, F. W. Zheng, B. T. Wang, P. Zhang, *J. Nucl. Mater.* **2013**, 441, 411.
- [7] J. T. Pegg, X. Aparicio-Angles, M. Storr, N. H. de Leeuw, *J. Nucl. Mater.* **2017**, 492, 269.
- [8] A. E. Shields, D. Santos-Carballal, N. H. de Leeuw, *J. Nucl. Mater.* **2016**, 473, 99.
- [9] B. Szpunar, J. A. Szpunar, *J. Nucl. Mater.* **2013**, 439, 243.
- [10] H. He, D. A. Andersson, D. D. Allred, K. D. Rector, *J. Phys. Chem. C* **2013**, 117, 16540.
- [11] M. Gajdos, K. Hummer, G. Kresse, J. Furthmüller, F. Bechstedt, *Phys. Rev. B* **2006**, 73, 045112.
- [12] X.-D. Wen, R. L. Martin, L. E. Roy, G. E. Scuseria, S. P. Rudin, E. R. Batista, T. M. McCleskey, B. L. Scott, E. Bauer, J. J. Joyce, T. Durakiewicz, *J. Chem. Phys.* **2012**, 137, 154707.

- [13] C. L. Dugan, G. G. Peterson, A. Mock, C. Young, J. M. Mann, M. Nastasi, M. Schubert, L. Wang, W.-N. Mei, I. Tanabe, P. A. Dowben, J. Petrosky, *Eur. Phys. J. B* **2018**, 91, 67.
- [14] A. Mock, C. Dugan, S. Knight, R. Korlacki, J. M. Mann, M. M. Kimani, J. C. Petrosky, P. A. Dowben, M. Schubert, *Appl. Phys. Lett.* **2019**, 114, 211901.
- [15] C. Mo, Y. Yang, W. Kang, P. Zhang, *Phys. Lett. A* **2016**, 380, 1481.
- [16] H. Shi, M. Chu, P. Zhang, *J. Nucl. Mater.* **2010**, 400, 151.
- [17] L. E. Roy, T. Durakiewicz, R. L. Martin, J. E. Peralta, G. E. Scuseria, C. G. Olson, J. J. Joyce, E. Guziewicz, *J. Comput. Chem.* **2008**, 29, 2288.
- [18] I. D. Prodan, G. E. Scuseria, R. L. Martin, *Phys. Rev. B* **2006**, 73, 045104/045110.
- [19] B. Dorado, B. Amadon, M. Freyss, M. Bertolus, *Phys. Rev. B* **2009**, 79, 235125.
- [20] S. L. Dudarev, D. Nguyen Manh, A. P. Sutton, *Philos. Mag. B* **1997**, 75, 613.
- [21] A. J. Devey, *J. Nucl. Mater.* **2011**, 412, 301.
- [22] P.-F. Sui, Z.-H. Dai, X.-L. Zhang, Y.-C. Zhao, *Chin. Phys. Lett.* **2015**, 32, 077101.
- [23] Q. Chen, X. Lai, T. Tang, B. Bai, M. Chu, Y. Zhang, S. Tan, *J. Nucl. Mater.* **2010**, 401, 118.
- [24] S. L. Dudarev, G. A. Botton, S. Y. Savrasov, Z. Szotek, W. M. Temmerman, A. P. Sutton, *Phys. Status Solidi A* **1998**, 166, 429.
- [25] G. Leinders, T. Cardinels, K. Binnemans, M. Verwerft, *J. Nucl. Mater.* **2015**, 459, 135.
- [26] R. Lasowski, G. K. H. Madsen, P. Blaha, K. Schwarz, *Phys. Rev. B* **2004**, 69, 140408R.
- [27] S. Joaquin, *Chem. Phys. Lett.* **1976**, 42, 131.
- [28] T. T. Meek, B. V. Roedern, *Vacuum* **2008**, 83, 226.
- [29] C. Kruschwitz, S. Mukhopadhyay, D. Schwellenbach, T. Meek, B. Shaver, T. Cunningham, J. P. Auxier, in *Hard X-Ray, Gamma-Ray, and Neutron Detector Physics XVI*, Proc. SPIE Vol. 9213 San Diego, Society of Photo-Optical Instrumentation Engineers, Bellingham, WA **2014**, p. 92130C.
- [30] J. Schoenes, *J. Appl. Phys.* **1978**, 49, 1463.
- [31] J. Schoenes, *Phys. Rep.* **1980**, 63, 301.
- [32] J. Schoenes, *J. Chem. Soc., Faraday Trans. 2* **1987**, 83, 1205.
- [33] W. Siekhaus, J. Crowhurst, *IOP Conf. Ser.: Mater. Sci. Eng.* **2010**, 9, 012055.
- [34] T. T. Meek, B. von Roedern, P. G. Clem, R. J. Hanrahan Jr., *Mater. Lett.* **2005**, 59, 1085.
- [35] M. Mann, D. Thompson, K. Serivalsatit, T. M. Tritt, J. Ballato, J. Kolis, *Cryst. Growth Des.* **2010**, 10, 2146.
- [36] C. Young, J. Petrosky, J. M. Mann, E. M. Hunt, D. Turner, P. A. Dowben, *J. Phys.: Condens. Matter* **2017**, 29, 035005.
- [37] T. D. Kelly, J. Petrosky, J. McClory, T. Zens, D. Turner, J. Mann, J. Kolis, J. A. Colón Santana, P. A. Dowben, *MRS Proc.* **2013**, 1576, mrrs13-1576-ww10-03.
- [38] T. Kelly, J. Petrosky, D. Turner, J. McClory, J. Mann, J. Kolis, X. Zhang, P. Dowben, *Phys. Status Solidi RRL* **2014**, 8, 283.
- [39] D. B. Turner, T. D. Kelly, G. R. Peterson, J. D. Reding, R. L. Hengehold, J. M. Mann, J. W. Kolis, P. A. Xin Zhang, *Phys. Status Solidi B* **2016**, 253, 1970.
- [40] C. Young, J. Petrosky, J. M. Mann, E. M. Hunt, D. Turner, T. Kelly, *Phys. Status Solidi RRL* **2016**, 10, 687.
- [41] S. Knight, R. Korlacki, C. Dugan, J. C. Petrosky, A. Mock, P. A. Dowben, J. M. Mann, M. M. Kimani, M. Schubert, *J. Appl. Phys.* **2020**, 127, 125103.
- [42] G. Kresse, J. Furthmüller, *Phys. Rev. B* **1996**, 54, 11169.
- [43] G. Kresse, J. Furthmüller, *Comput. Mater. Sci.* **1996**, 6, 15.
- [44] G. Kresse, J. Hafner, *Phys. Rev. B* **1993**, 47, 558.
- [45] G. Kresse, D. Joubert, *Phys. Rev. B* **1999**, 59, 1758.
- [46] J. P. Perdew, K. Burke, M. Ernzerhof, *Phys. Rev. Lett.* **1996**, 77, 3865.
- [47] a) J. Heyd, G. E. Scuseria, M. Ernzerhof, *J. Chem. Phys.* **2003**, 118, 8207; b) Erratum, *J. Chem. Phys.* **2006**, 124, 219906.
- [48] H. Ehrenreich, M. H. Cohen, *Phys. Rev.* **1959**, 115, 786.
- [49] M. Gajdoš, K. Hummer, K. Kresse, J. Furthmüller, F. Bechstedt, *Phys. Rev. B* **2006**, 73, 045112.
- [50] B. Dorado, G. Jonard, M. Freyss, M. Bertolus, *Phys. Rev. B* **2010**, 82, 035114.
- [51] M. Iwasawa, Y. Chen, Y. Kaneta, T. Ohnuma, H.-Y. Geng, M. Kinoshita, *Mater. Trans.* **2006**, 47, 2651.
- [52] O. D. Jayakumar, I. K. Gopalakrishnan, A. Vinu, A. Asthana, A. K. Tyagi, *J. Alloys Compd.* **2008**, 461, 608.
- [53] T. Maehira, T. Hotta, *J. Magn. Magn. Mater.* **2007**, 310, 754.
- [54] P. J. Kelly, M. S. S. Brooks, *J. Chem. Soc., Faraday Trans. 2* **1987**, 83, 1189.
- [55] Y. Baer, J. Schoenes, *Solid State Commun.* **1980**, 33, 885.
- [56] L. Lynds, W. Young, J. Mohl, G. Libowitz, *Nonstoichiometric Compounds*, American Chemical Society, Washington, DC **1963**, pp. 58–65.
- [57] B. C. Frazer, G. Shirane, D. E. Cox, C. E. Olsen, *Phys. Rev.* **1965**, 140, A1448.
- [58] A. Padel, Ch de Novion, *J. Nucl. Mater.* **1969**, 33, 40.
- [59] K. Ikushima, S. Tsutsui, Y. Haga, H. Yasuoka, R. E. Walsteadt, N. M. Masaki, A. Nakamura, S. Nasu, Y. Onuki, *Phys. Rev. B* **2001**, 63, 104404.